The classical Coulomb three-body problem in the collinear eZe configuration

2004 J. Phys. A: Math. Gen. 37 803

(http://iopscience.iop.org/0305-4470/37/3/018)

INSTITUTE OF PHYSICS PUBLISHING JOURNAL OF PHYSICS A: MATHEMATICAL AND GENERAL

J. Phys. A: Math. Gen. **37** (2004) 803–822 PII: S0305-4470(04)67287-8

The classical Coulomb three-body problem in the collinear eZe configuration

Mitsusada M Sano

Graduate School of Human and Environmental Studies, Kyoto University, Sakyo, Kyoto, 606-8501, Japan

Received 6 August 2003, in final form 24 September 2003
Published 7 January 2004
Online at stacks.iop.org/JPhysA/37/803 (DOI: 10.1088/0305-4470/37/3/018)

Abstract

We investigate the classical dynamics of a two-electron atom and ions H^-, He, Li^+, Be^{2+}, ..., in the collinear eZe configuration. We consider the case that the masses of all particles are finite. It is revealed that the mass ratio ξ between the nucleus and electron plays an important role for the dynamical behaviour of these systems. With the aid of an analytical tool and numerical computation, it is shown that, thanks to a large mass ratio ξ, the classical dynamics of these systems is fully chaotic, probably hyperbolic. Experimental evidence of this finding is also proposed.

PACS numbers: 45.50.Jf, 05.45.−a, 05.45.Mt, 31.10.+z

(Some figures in this article are in colour only in the electronic version)

1. Introduction

The three-body problem in celestial mechanics is one of the pioneer studies on chaotic phenomena and, at the same time, one of the oldest and the most famous problems in physics. The first systematic work was carried out by Poincaré, for which he won the prize established by King Oscar II of Sweden and Norway (Poincaré 1899). The main result of his work is that the motion of three particles is very complicated (i.e. what we now call 'chaos') and thus it is generally hard to solve it practically. After Poincaré, many mathematicians and physicists contributed to this problem; see, for instance, the book by Siegel and Moser (1971) in the mathematical literature. In addition, the innovation of computers has assisted physicists in their investigation of this problem. However, our understanding of the three-body problem is far from complete. The investigation is still ongoing.

The three-body problem also exists in Coulomb systems. The most popular Coulomb three-body system is the helium atom which consists of one nucleus and two electrons. In the early stage of quantum mechanics, many physicists did not know what to do with the spectrum of the helium atom, in spite of the successful explanation of the spectrum of the hydrogen atom. For the hydrogen atom, the stable periodic orbits correspond to its eigenenergies. This

correspondence is now called the Bohr–Sommerfeld (BS) quantization. However, it was not possible to explain the spectrum of the helium atom using the BS quantization scheme. Einstein extended the BS quantization to the higher-dimensional classically integrable case—which we now call the Einstein–Brillouin–Keller (EBK) quantization—and pointed out indirectly this problem of the helium atom (i.e. non-integrable case) referring to the work by Poincaré (Einstein 1917). About 50 years later, Gutzwiller succeeded in deriving an approximate quantization condition for hyperbolic cases. His formula expresses the density of states in terms of unstable periodic orbits, which is now called the Gutzwiller trace formula (Gutzwiller 1971, 1990). In the early 1990s, several physicists applied the Gutzwiller trace formula to the hydrogen negative ion (Gaspard and Rice 1993) and helium atom (Ezra *et al* 1991) in collinear configuration, i.e. the restricted Coulomb three-body problem. A series of these studies showed that these atoms and ions in the collinear eZe configuration are fully chaotic, probably hyperbolic and the Gutzwiller trace formula yields good approximate values for a series of eigenenergies with angular momentum $\mathbf{L} = 0$ numerically; see also the review by Tanner *et al* (2000). Here 'e' and 'Z' represent the electron and nucleus, respectively. Thus, 'eZe' denotes the order of particles on a line. Their work has left a question as to the why hydrogen negative ion and helium atom the in collinear eZe configuration are fully chaotic. We have used the term 'fully chaotic' to mean that almost all periodic orbits are hyperbolic. Thus, we have used the term 'fully chaotic' for the system which is almost chaotic, but possesses a small tiny island. In addition, we shall use the term 'hyperbolic' to mean that all periodic orbits are hyperbolic.

It has been shown numerically that if the mass of the nucleus is infinite for the eZe collinear configuration, the symbolic description of it is complete for the negative energy $E < 0$ and $Z \geqslant 1$ (Bai *et al* 1998). This result suggests that, for the infinite nucleus mass, the dynamics is hyperbolic.

In this paper, we consider the case that all masses are finite and we numerically confirm that the dynamics of a two-electron atom and ions in the collinear eZe configuration, i.e. H^-, He, Li^+, Be^{2+}, ..., is hyperbolic. Parameters of these systems are the mass ratio $\xi = m_n/m_e$ and the charge Z of the nucleus, where m_n and m_e are the masses of the nucleus and electron, respectively. We employ a numerical computation for these systems with the aid of an analytical tool—the triple collision manifold (TCM; McGehee 1974)—and symbolic dynamics (Tanikawa and Mikkola 2000) from celestial mechanics. The TCM is a manifold which is a set of the initial or final conditions of the triple collision orbit, i.e. thus just the triple collision points. The flow on the TCM does not have physical reality, because the TCM corresponds to just triple collisions. However, the flow on the TCM affects the flow near the TCM because of the continuous property of the solution for the equations of motion. Thus, we can study the behaviour near the triple collision from the flow on the TCM. It is shown that the mass ratio ξ plays an important role for the dynamical behaviour of these systems. To be precise, a sufficiently large mass ratio ξ makes the system fully chaotic. Therefore, it is revealed that all of these systems are fully chaotic, probably hyperbolic, since the mass ratio is sufficiently large, e.g. $m_p/m_e \approx 1840$, where m_p is the mass of the proton.

We confirm this result as follows. First, we elucidate the ξ dependence of the local structure near the triple collision by examining the flow on the TCM. In particular, we investigate the stable (or unstable) manifold of two critical points on the TCM. By this analysis, we show the change of the triple collision orbit when ξ is increased. Let us denote the winding number of the stable (or unstable) manifold (on the TCM) of the critical point around the body of the TCM by $\mathcal{N}$. Later we shall define the body of the TCM precisely. It is shown that when $\xi \to 0$, $\mathcal{N}$ becomes infinite and, in the opposite limit, when ξ is increased, $\mathcal{N}$ is decreased and saturated to certain values. Secondly, we examine the morphology of the

Poincaré surface of section using the associated symbolic dynamics. The symbolic dynamics is naturally introduced by labelling the double collision between the particles 1 and 2 (2 and 3) by symbol 1 (2). The position of the triple collision orbits on the Poincaré surface of section is specified. When $(Z, \xi) = (1, 1)$, there is a torus on the Poincaré surface of section, whose corresponding sequence of symbols is $\ldots 12121212 \ldots$. The triple collision orbits form curves on the Poincaré surface of section. We call these curves the triple collision curves, $\mathcal{C}_{\mathrm{TC}}$. In this case, $\mathcal{C}_{\mathrm{TC}}$ crosses its reversed pair $\mathcal{C}^t_{\mathrm{TC}}$ transversely except near the torus. $\mathcal{C}^t_{\mathrm{TC}}$ is mapped to $\mathcal{C}_{\mathrm{TC}}$ by the symmetry operation due to the reverse operation. For helium $(Z, \xi) = (1, 4m_p/m_e)$, there is no torus. $\mathcal{C}_{\mathrm{TC}}$ crosses its pair $\mathcal{C}^t_{\mathrm{TC}}$ transversely everywhere. From numerical calculation, $\mathcal{C}_{\mathrm{TC}}$ and $\mathcal{C}^t_{\mathrm{TC}}$ are parallel to the stable and unstable manifolds, respectively, in the Poincaré section for the Poincaré map. Therefore, this fact is strong evidence that the stable and unstable manifolds transversely cross each other for the case of helium in the collinear eZe configuration. In addition, we show the relationship between the structure of the stable and unstable manifolds of two critical points on the TCM and $\mathcal{C}_{\mathrm{TC}}$ and $\mathcal{C}^t_{\mathrm{TC}}$ on the Poincaré section. At this time, it is found that the change of the triple collision orbit on the TCM w.r.t. ξ is related to the collapse of the torus whose corresponding symbol sequence is $\ldots 12121212 \ldots$. The above facts strongly suggest that the two-electron atom and ions in the collinear eZe configuration are fully chaotic, probably hyperbolic.

The organization of this paper is as follows. In section 2, we introduce the Hamiltonian of the systems considered in this paper. Due to the attractive interaction between neighbouring particles, double collisions surely occur. Therefore, a regularization is required before numerical computation. We choose an algorithmic regularization, not an analytical regularization such as a Kustaanheimo–Stiefel transformation or a Levi-Civita transformation. In section 3, the TCM is introduced. The ξ dependence of the flow on the TCM is numerically investigated. In particular, the change of the triple collision orbit w.r.t. ξ is shown. In section 4, the method of symbolic dynamics is applied to the systems for the case $Z = 1$ and $\xi = 1$ and the case of helium. In the former case, there is a torus whose symbol sequence is $\ldots 12121212 \ldots$. We examine the topological character of this system in detail. On the other hand, in the case of helium, there is no torus whose corresponding symbol sequence is $\ldots 12121212 \ldots$. In fact, the corresponding orbit for the symbol sequence $\ldots 12121212 \ldots$ is an isolated unstable periodic orbit. With the result of section 3, we consider what this observation means. In section 5, the results of this paper are summarized.

2. Hamiltonian and regularization

We consider three particles 1, 2 and 3 whose masses are $m_1 = m_e, m_2 = m_n = \xi m_e$ and $m_3 = m_e$ and whose charges are $-e$, Ze and $-e$, respectively. The mass ratio ξ is given by $\xi = m_n/m_e$. The Hamiltonian for this system is

$$H = \sum_{i=1}^{3} \frac{p_i^2}{2m_i} - \frac{Ze^2}{|q_1 - q_2|} - \frac{Ze^2}{|q_2 - q_3|} + \frac{e^2}{|q_1 - q_3|}. \tag{1}$$

Now we employ the famous scaling for Coulomb systems

$$q_i = \alpha q_i' \qquad p_i = \beta p_i' \qquad E = \gamma E' \tag{2}$$

with

$$\alpha = \frac{Z}{m_e e^2 |E|} \qquad \beta = |E|^{1/2} m_e e^2 \qquad \gamma = m_e e^4. \tag{3}$$

E is the value of the Hamiltonian H. After this scaling, we obtain the following Hamiltonian:

$$\mathcal{H} = \frac{p_1'^2}{2} + \frac{p_2'^2}{2\xi} + \frac{p_3'^2}{2} - \frac{1}{|q_1' - q_2'|} - \frac{1}{|q_2' - q_3'|} + \frac{1}{Z|q_1' - q_3'|} = E' = -1. \tag{4}$$

For simplicity, we set $E' = -1$. Now the particles are arranged in the order $q_1' \leqslant q_2' \leqslant q_3'$. If we set $(Z, \xi) = (-1, 1)$, the system is equivalent to the system which was investigated in the gravitational three-body problem (Tanikawa and Mikkola 2000). We set the total momentum to be zero and change the variables q_i' to

$$Q_1 = q_2' - q_1' \qquad Q_2 = q_2' \qquad Q_3 = q_3' - q_2' \tag{5}$$

with new momenta

$$P_1 = -p_1' \qquad P_2 = p_1' + p_2' - p_3' \qquad P_3 = p_3'. \tag{6}$$

This canonical transformation is generated by the following generating function W:

$$W = P_1(q_2' - q_1') + P_2 q_2' + P_3(q_3' - q_2'). \tag{7}$$

The final form of the Hamiltonian $\mathcal{H}$ is

$$\mathcal{H} = \frac{P_1^2}{2\mu} + \frac{P_2^2}{2\mu} - \frac{P_1 P_2}{\xi} - \frac{1}{Q_1} - \frac{1}{Q_2} + \frac{1}{Z(Q_1 + Q_2)} = -1 \tag{8}$$

with $\mu = \xi/(\xi + 1)$. After the canonical transformation, we replace (P_3, Q_3) by (P_2, Q_2) for convenience. The parameters of this Hamiltonian are the charge Z and the mass ratio ξ.

The potential in equation (8) has singularities associated with double collisions of particles. Thus, an appropriate regularization is needed. To regularize them, in celestial mechanics a transformation such as the Kustaanheimo–Stiefel transformation or the Levi-Civita transformation is usually employed. However, an algorithmic regularization (Mikkola and Tanikawa 1999) is used here. The merit of this choice is that for accurate numerical integration of equations of motion, the symplectic integrator method can be used (Yoshida 1990). For the usual analytical regularization, the symplectic integrator method cannot be applied, since there are coupling terms of position and momentum in the Hamiltonian, i.e. the Hamiltonian after the transformation mentioned above is not a summation of the form $\mathcal{H} = T(\mathbf{P}) + V(\mathbf{Q})$. We will use the sixth-order symplectic integrator method in section 4. After regularization, double collision is extended to just elastic collision and the triple collision is not regularized in general. The interaction between outer and middle particles is attractive, while the interaction between outer particles is repulsive. Thus, neighbouring particles are always attracted and collide with each other. Hence the trajectory of three particles is, in general, a sequence of collisions. Among collisions, triple collisions exist as very rare events. In fact, the measure of the set of triple collisions would be zero. However, triple collisions form the bone structure of the dynamics of our systems which we will see in sections 3 and 4.

Here the symbolic coding of the orbit which will be extensively used in section 4 is introduced briefly. Let us denote the whole set of orbits in our systems by $\mathcal{O}$. The set $\mathcal{O}$ is a union of $\mathcal{O}_{\mathrm{DC}}$ and $\mathcal{O}_{\mathrm{TC}}$, where $\mathcal{O}_{\mathrm{DC}}$ is the set of orbits which only consist of double collisions and $\mathcal{O}_{\mathrm{TC}}$ is the set of orbits which include triple collisions:

$$\mathcal{O} = \mathcal{O}_{\mathrm{DC}} \cup \mathcal{O}_{\mathrm{TC}}. \tag{9}$$

For an orbit of $\mathcal{O}_{\mathrm{DC}}$, it is natural that the double collision with the particles 1 and 2 (2 and 3) is labelled by symbol 1 (2). Therefore, the symbol set for $\mathcal{O}_{\mathrm{DC}}$ is $\mathbf{A}_0 = \{1, 2\}$. Let us express a given orbit of $\mathcal{O}_{\mathrm{DC}}$ as a sequence of symbols as follows

$$\mathbf{n} = \ldots n_{-2} n_{-1} \cdot n_0 n_1 n_2 \ldots, \tag{10}$$

where $n_i \in \mathbf{A}_0, i \in \mathbf{Z}$. In order to describe an orbit of $\mathcal{O}_{\mathrm{TC}}$ as a symbol sequence, we need another symbol, i.e. 0. We set $\mathbf{A} = \{0, 1, 2\}$. The triple collision orbit is started and/or ended by the triple collision. Let us label the triple collision by the symbol 0. The orbit which experiences the triple collision cannot be continued. Thus, we regard as 0 continuing endlessly after the first 0 in the future and before the last 0 in the past, if 0 appears in the sequence. For example, a triple collision orbit is represented as

$$\mathbf{n} = \ldots 000 n_{-l} n_{-(l-1)} \ldots n_{-1} \cdot n_0 n_1 n_2 \ldots, \tag{11}$$

or

$$\mathbf{n} = \ldots n_{-3} n_{-2} n_{-1} \cdot n_0 n_1 \ldots n_m 000 \ldots, \tag{12}$$

or

$$\mathbf{n} = \ldots 000 n_{-l} n_{-(l-1)} \ldots n_{-1} \cdot n_0 n_1 \ldots n_m 000 \ldots, \tag{13}$$

where $n_i \in \mathbf{A}_0$. The shift operator σ on $\mathbf{A}^{\mathbf{Z}}$ is defined by

$$\sigma(\ldots n_{-2} n_{-1} \cdot n_0 n_1 n_2 \ldots) = \ldots n_{-2} n_{-1} n_0 \cdot n_1 n_2 \ldots. \tag{14}$$

We sometimes call the finite symbol sequence the 'word'. For instance, 12 and 1211 are words.

3. Triple collision manifold

Triple collisions are, in general, essential singularities and thus are not regularized. They are rare events. Therefore, it is hard to visualize triple collisions. In order to investigate the structure near the triple collision, a technical method is required. For the celestial problem, McGehee (1974) has developed such a method. He has derived the equations of motion for the flow just on the triple collision. Its derivation is a successive application of tricky transformations to the equations of motion (4) and the energy conservation relation $\mathcal{H} = T(\mathbf{p}) - U(\mathbf{q}) = E$. A manifold on which the orbit experiences just the triple collision is obtained by setting the moment of inertia to be zero (i.e. just triple collision) in the final energy conservation relation. This substitution is meaningful owing to tricky transformations (i.e. scalings and time transformations). This manifold is called the TCM. Thanks to the similarity between the celestial problem and the Coulomb problem, this method can also be applied to our Coulomb problem. Since the transformations are tricky and complicated, in order to be self-contained, we show the derivation of it briefly in the appendix. For the details of the derivation, we recommend that readers consult the paper by McGehee (1974). Starting from the energy conservation equation (4) and the equations of motion (4), after lengthy calculation (i.e. six changes of variables), we obtain the energy conservation relation with $r = 0$, i.e. the moment of inertia $r^2 = q_1^2 + \xi q_2^2 + q_3^2$ is zero (just the triple collision) or, alternatively, with the total energy $E = 0$:[1]

$$w^2 + s^2 - 1 + (1 - s^2)^2 W(s)^{-1} v^2 = 0. \tag{15}$$

Equation (15) defines a surface in (s, v, w)-coordinates, i.e. the TCM. The TCM is topologically equivalent to a sphere with four holes. A schematic picture for the TCM is depicted in figure 1. For the definitions of s, v, w and $W(s)$, see the appendix. We only explain what s represents. s represents the configuration of three particles. s is valued in

[1] r and E appear as a term rE in the energy relation and equations of motion (see the appendix). Therefore, the TCM and the flow on the TCM are the same for either $r = 0$ and $E = 0$.

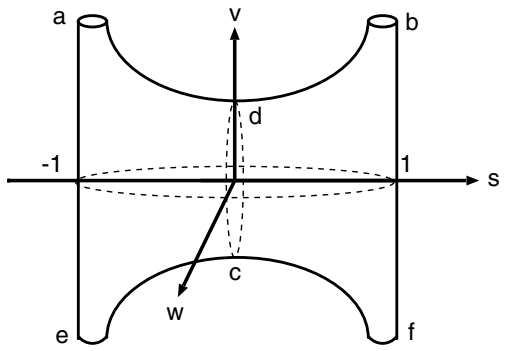

Figure 1. The triple collision manifold: there are two critical points c and d.

$[-1, 1]$. $s = -1$ ($s = 1$) corresponds to the double collision between the particles 1 and 2 (2 and 3). The flow on the TCM is determined by the following equations of motion:

$$\begin{aligned}
\frac{dv}{d\tau} &= \frac{\lambda}{2} W(s)^{1/2} \left[1 - \frac{1-s^2}{W(s)} v^2 \right] \\
\frac{ds}{d\tau} &= w \\
\frac{dw}{d\tau} &= -s + \frac{2s(1-s^2)}{W(s)} v^2 + \frac{1}{2} \frac{W'(s)}{W(s)} (1 - s^2 - w^2) - \frac{\lambda}{2} \frac{1-s^2}{W(s)^{1/2}} vw.
\end{aligned} \tag{16}$$

For the definitions of λ, s, v, w and τ, see the appendix. There are two critical points $c = (0, -v_c, 0)$ and $d = (0, v_c, 0)$, two infinite arms (a and b), and two infinite legs (e and f), where $v_c = W(0)^{1/2}$. Most of orbits on the TCM come from infinity of one of two legs winding around it and go out to infinity of one of two arms winding around it.

There is an important property for the orbits with $r \neq 0$ (i.e. for total flow).

Property 3.1. *For $\mathcal{H} = E < 0$, the orbits run inside the TCM, i.e. $w^2 + s^2 + (1 - s^2)^2 W(s)^{-1} v^2 \leqslant 1$. On the other hand, for $\mathcal{H} = E > 0$, the orbits run outside the TCM, i.e., $w^2 + s^2 + (1 - s^2)^2 W(s)^{-1} v^2 \geqslant 1$. For $\mathcal{H} = E = 0$, the orbits run on the TCM, i.e., $w^2 + s^2 + (1 - s^2)^2 W(s)^{-1} v^2 = 1$.*

Hereafter, we consider the case of $\mathcal{H} = E < 0$.

If the orbit crosses $s = -1$ ($s = 1$), the corresponding trajectory in the configuration space experiences the double collision between the particles 1 and 2 (2 and 3) with the symbol 1 (2). After some collisions, they go out to infinity by changing its binary or not. There also exist the triple collision orbits. By definition, the triple collision orbits are the orbits which start/end at the TCM (i.e. $r = 0$). This means that the triple collision orbit cannot be regularized; that is, the triple collision orbits cannot continue after/before the triple collisions. As shown by McGehee (1974), the triple collision orbits form one parameter family. This fact is understood from the stability analysis of the critical points c and d. The critical points c and d are the fixed points of the flow equation (16). At the same time, they are the fixed points of the total flow equation (A.21) which is not restricted to $r = 0$. The stability analysis of the fixed points c and d shows that $\dim(\mathcal{W}^s(c)) = 2$, $\dim(\mathcal{W}^u(c)) = 1$ and $\dim(\mathcal{W}^s(d)) = 1$, $\dim(\mathcal{W}^u(d)) = 2$, where $\mathcal{W}^s(x)$ and $\mathcal{W}^u(x)$ are the stable and unstable manifolds of x, respectively. Figure 2 shows a schematic picture of $\mathcal{W}^s(c)$, $\mathcal{W}^u(c)$, $\mathcal{W}^s(d)$ and $\mathcal{W}^u(d)$. One branch of $\mathcal{W}^s(c)$ (which we call $\mathcal{W}^{s,*}(c)$) comes into c on the TCM from the outside of the TCM (i.e. $r \neq 0$) along

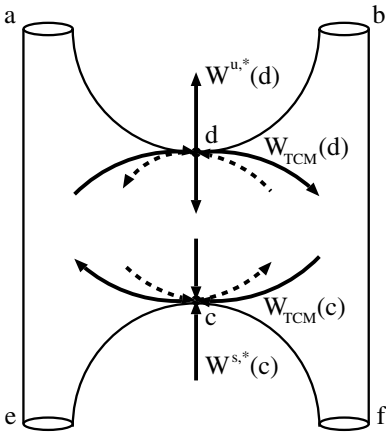

Figure 2. The schematic picture of the stable and unstable manifolds of the critical points c and d: $\mathcal{W}(c)$ and $\mathcal{W}(d)$ are depicted. $\dim(\mathcal{W}^s(c)) = 2, \dim(\mathcal{W}^u(c)) = 1, \dim(\mathcal{W}^s(d)) = 1, \dim(\mathcal{W}^u(d)) = 2$.

the v-axis. Similarly, one branch of $\mathcal{W}^u(d)$ (which we call $\mathcal{W}^{u,*}(d)$) goes out of d on the TCM to the outside of the TCM (i.e. $r \neq 0$) along the v-axis. The other branch of $\mathcal{W}^s(c)$ and $\mathcal{W}^u(c)$ (which we call $\mathcal{W}_{\rm TCM}(c)$) runs on the TCM and winds around the TCM. Similarly, the other branch of $\mathcal{W}^u(d)$ and $\mathcal{W}^s(d)$ (which we call $\mathcal{W}_{\rm TCM}(d)$) runs on the TCM and winds around the TCM. In the outside of the TCM (i.e. $r \neq 0$) near the critical points c and d, there exists one parameter family of the orbits which approach $\mathcal{W}_{\rm TCM}(c)$ as $\tau \to \infty$. Similarly, there exists one parameter family of the orbits which escape from $\mathcal{W}_{\rm TCM}(d)$ as $\tau \to \infty$. Therefore, $\mathcal{W}_{\rm TCM}(c)$ and $\mathcal{W}_{\rm TCM}(d)$ determine the behaviour of the triple collision orbits. Unfortunately, this discussion here is limited to the neighbourhood of the critical points c and d (i.e. local property). In the next section, we investigate $\mathcal{W}_{\rm TCM}(c)$ and $\mathcal{W}_{\rm TCM}(d)$ numerically to show the global topological property of the triple collision orbits. For later use, we call the part of the TCM between two critical points c and d the body of the TCM, to be precise, $\{(s, v, w); -v_c \leqslant v \leqslant v_c, (s, v, w)$ on the TCM$\}$.

Our interest in this section is focused on the ξ dependence of the flow on the TCM. In the celestial problem in the collinear configuration considered in section 10 of the paper by McGehee (1974), it is shown that for the case of $m_1 = m_3 = m$ and $m_2 = \epsilon m$, when $\epsilon \to 0$, the orbits on the TCM wind around the TCM infinitely. Thanks to the similarity between the celestial problem and the Coulomb problem, for our Coulomb systems, the same argument is easily shown following the discussion of McGehee (1974).

Property 3.2. *When $\xi \to 0$, the orbits on the TCM wind around the body of the TCM infinitely often.*

This is due to the fact that $\mathrm{d}v/\mathrm{d}\tau \to 0$ as $\xi \to 0$. The proof is the same as proposition 10.1 of McGehee (1974).

In order to show the ξ dependence of the flow on the TCM for large ξ, we numerically calculate $\mathcal{W}_{\rm TCM}(c)$ and $\mathcal{W}_{\rm TCM}(d)$. For this numerical integration of equation (16), we use the fourth-order Runge–Kutta method. Figure 3 depicts $\mathcal{W}_{\rm TCM}(c)$ and $\mathcal{W}_{\rm TCM}(d)$ for $(Z, \xi) = (1, 1)$. Figures 4(a) and (b) depict one branch (the unstable manifold) of $\mathcal{W}_{\rm TCM}(c)$ for the cases $(Z, \xi) = (1, 0.1)$ and $(1, 6)$, respectively. The change of $\mathcal{W}_{\rm TCM}(c)$ w.r.t. ξ is clearly seen in figure 4. When ξ is increased, the winding number $\mathcal{N}$ of $\mathcal{W}_{\rm TCM}(c)$ or $\mathcal{W}_{\rm TCM}(d)$

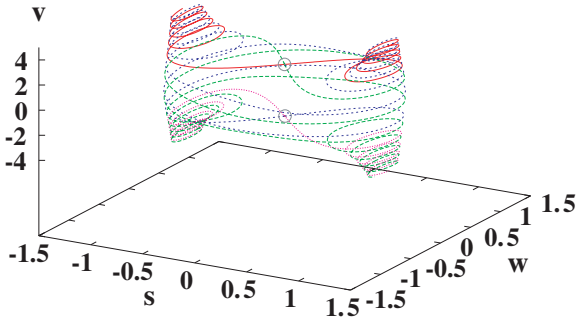

Figure 3. The stable and unstable manifolds of the critical points c and d on the TCM for $(Z, \xi) = (1, 1)$: $\mathcal{W}_{\mathrm{TCM}}(c)$ and $\mathcal{W}_{\mathrm{TCM}}(d)$. Two circles indicate the positions of two critical points c and d.

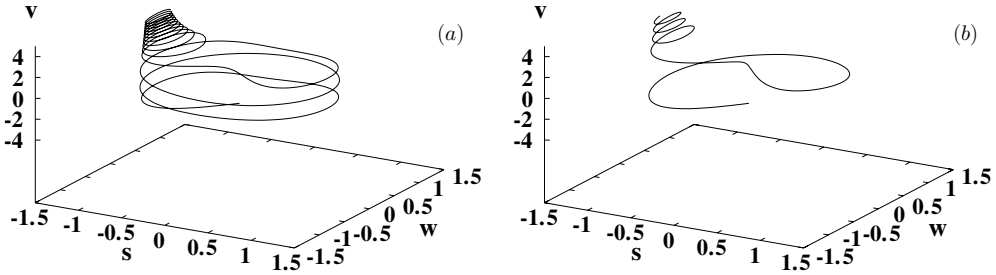

Figure 4. The unstable manifold of the critical point c on the TCM: (a) $(Z, \xi) = (1, 0.1)$, (b) $(Z, \xi) = (1, 6)$.

around the body of the TCM is decreased. Although further ξ is increased from $\xi = 6$, further change does not occur. Thus, when ξ increases, $\mathcal{N}$ monotonically decreases to a certain value. This property is also observed for different values of Z.

Remark. For our Coulomb system, the potential part of the Hamiltonian does not include the masses. Thus, v_c is independent of ξ. For the gravitational case, the TCM has the same topology compared with our Coulomb system. However, the potential part of the Hamiltonian includes the masses. This makes a difference in the behaviour of the flow on the TCM. If $m_1 = 1, m_2 = \xi$ and $m_3 = 1$, $v_c \sim \sqrt{\xi}$ as $\xi \to \infty$. Therefore, when $\xi \to \infty$, the winding number of $\mathcal{W}_{\mathrm{TCM}}(c)$ or $\mathcal{W}_{\mathrm{TCM}}(d)$ may not decrease as well as in the case of our Coulomb system. Thus, it is supposed that, in the gravitational three-body problem in the collinear configuration, the system hardly becomes hyperbolic, namely it always has stable orbits (i.e. tori).

To summarize, when $\xi \to 0$, the orbit on the TCM winds around the body of the TCM infinitely often. When ξ is increased, the number of times that the orbit winds around the body of TCM is monotonically decreased to a certain value. The latter fact is related to what we examine in the next section.

4. Symbolic dynamics

In this section, we examine the global structure of the Poincaré surface of section by using the associated symbolic dynamics. The Poincaré surface of section is defined as follows. We

denote the position on the line $Q_1 = Q_2$ in the (Q_1, Q_2) plane by R, i.e. $R = Q_1 = Q_2$. On this line, the momenta P_1 and P_2 are specified by new variables θ and R

$$P_1 = \sqrt{T}\cos\theta + \sqrt{\frac{\xi T}{\xi + 2}}\sin\theta \qquad P_2 = \sqrt{T}\cos\theta - \sqrt{\frac{\xi T}{\xi + 2}}\sin\theta \tag{17}$$

where T is the kinetic part of the total energy. Our surface of section is the (θ, R) plane where $0 \leqslant R \leqslant R_{\max}$, $0 \leqslant \theta < 2\pi$ and $R_{\max} = 2 - 1/2Z$. We denote this plane by $\mathcal{D}$. We define the map χ from the point $\mathbf{z} \in \mathcal{D}$ to the bi-infinite symbol sequence $\mathbf{n}$ which is an itinerary of the orbit started from $\mathbf{z}$ at the time zero:

$$\begin{array}{rccl} \chi : & \mathcal{D} & \to & \mathbf{A}^{\mathbf{Z}} \\ & \mathbf{z} & \mapsto & \mathbf{n} = \ldots n_{-2}n_{-1} \cdot n_0 n_1 n_2 \ldots . \end{array} \tag{18}$$

We define the map $\chi^{(+)}$ from the point $\mathbf{z}$ to the semi-infinite symbol sequence $\mathbf{n}^{(+)}$:

$$\begin{array}{rccl} \chi^{(+)} : & \mathcal{D} & \to & \mathbf{A}^{\mathbf{N}} \\ & \mathbf{z} & \mapsto & \mathbf{n}^{(+)} = n_{-1} \cdot n_0 n_1 n_2 \ldots . \end{array} \tag{19}$$

We also consider the following map Ξ_l from the semi-infinite symbol sequence to the finite symbol sequence with length $l + 2$:

$$\Xi_l(n_{-1} \cdot n_0 n_1 \ldots) = n_{-1} \cdot n_0 n_1 \ldots n_l. \tag{20}$$

Let us introduce

$$\begin{aligned} \mathcal{D}_1 &= \{(\theta, R) : 0 \leqslant \theta < \pi, 0 \leqslant R \leqslant R_{\max}\} \\ \mathcal{D}_2 &= \{(\theta, R) : \pi \leqslant \theta < 2\pi, 0 \leqslant R \leqslant R_{\max}\}. \end{aligned} \tag{21}$$

There are two symmetry operations on $\mathcal{D}$: (1) if the orbit starting $\mathbf{z} = (\theta, R) \in \mathcal{D}_1$ has the symbol sequence $\ldots m_{-2}m_{-1} \cdot n_0 n_1 \ldots$, then $\ldots n_1 n_0 \cdot m_{-1}m_{-2} \ldots$ is a symbol sequence for the point $(2\pi - \theta, R) \in \mathcal{D}_2$; (2) if is the future symbol sequence corresponding to the orbit starting at $(\theta, R) \in \mathcal{D}_1$ and if $\cdot m_1 m_2 m_3 \ldots$ is the future symbol sequence corresponding to the orbit starting at $(\pi - \theta, R) \in \mathcal{D}_1$, then $\ldots m'_3 m'_2 m'_1 \cdot n_1 n_2 n_3 \ldots$ is the bi-infinite sequence corresponding to the full orbit starting at the point $(\theta, R) \in \mathcal{D}_1$, where $m'_i = 1$ if $m_i = 2$ and $m'_i = 2$ if $m_i = 1$. Thanks to these two symmetry operations, in order to investigate the global structure of $\mathcal{D}$, it is sufficient to study only the future orbits for the points in $\mathcal{D}_1$.

We numerically construct the map $\chi^{(+)}$ in the following way. We consider the rectangular lattice whose lattice size is 1800×1000 for $\mathcal{D}_1$. For each lattice point $\mathbf{z}_{nm}$, $1 \leqslant n \leqslant 1800$, $1 \leqslant m \leqslant 1000$, we numerically obtain the truncated symbol sequence $\Xi_{60}(\chi^{(+)}(\mathbf{z}_{nm}))$ by integrating the equations of motion for the Hamiltonian equation (8) using the sixth-order symplectic integrator method as mentioned in section 2.

As established for the celestial problem (Tanikawa and Mikkola 2000), the following properties are also true for our Coulomb system.

Property 4.1. *A trajectory in the (Q_1, Q_2) plane transversely crosses the line $Q_1 = Q_2$ except at $(\theta, R) = (0, 0)$, if it does at all.*

Property 4.2. *If a trajectory crosses the line $Q_1 = Q_2$ on the (Q_1, Q_2) plane, a double collision occurs before the trajectory again crosses it.*

The proof for the above properties is the same as in Tanikawa and Mikkola (2000).

From property 4.2, if we put the initial condition $\mathbf{z}$ in $\mathcal{D}_1$ whose trajectory crosses the line $Q_1 = Q_2$, then the corresponding orbit has the symbol sequence $\ldots n_{-3}n_{-2}1 \cdot 2n_1 n_2 \ldots$, where $n_i \in \mathbf{A}$.

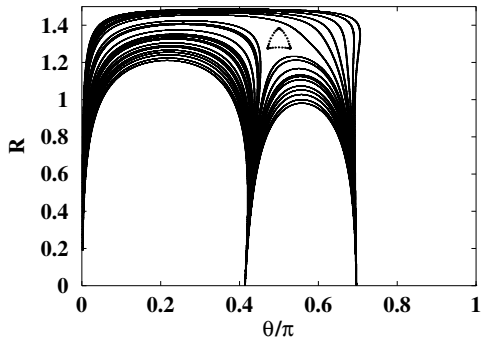

Figure 5. The triple collision curves $\mathcal{C}_{\rm TC}$ for the case of $(Z, \xi) = (1, 1)$: we also plot the torus region (triangle area). The curves are obtained by the symbol sequences with length 7 in future.

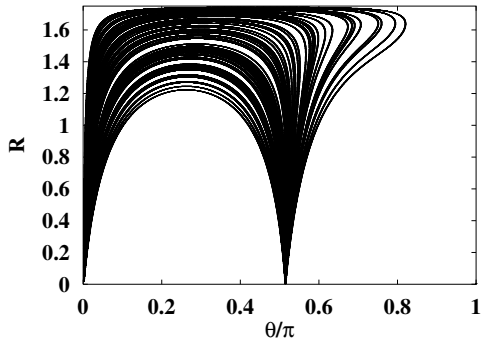

Figure 6. The triple collision curves $\mathcal{C}_{\rm TC}$ for the case of helium: the curves are obtained by the symbol sequences with length 7 in future.

The following two facts are numerically checked for our Coulomb systems (i.e. the case of $(Z, \xi) = (1, 1)$ and the case of the helium) as observed for the celestial problem (Tanikawa and Mikkola 2000). The plane $\mathcal{D}_1$ is divided into two regions of the points $\mathbf{z}$ having $\Xi_1(\chi^{(+)}(\mathbf{z})) = 1 \cdot 22$ and $1 \cdot 21$. Furthermore, it is divided into four regions of the points $\mathbf{z}$ having $\Xi_2(\chi^{(+)}(\mathbf{z})) = 1 \cdot 222, 1 \cdot 221, 1 \cdot 212$ and $1 \cdot 211$. This procedure is repeatedly applied. Then $\mathcal{D}_1$ is divided into smaller regions. The second fact is that the boundaries of regions of different symbol sequences form curves in $\mathcal{D}_1$. It turns out that these curves are initial conditions of orbits which end in triple collision. So we call these curves the triple collision curves. We denote them by $\mathcal{C}_{\rm TC}$.

Figures 5 and 6 depict the triple collision curves $\mathcal{C}_{\rm TC}$ for the case of $(Z, \xi) = (1, 1)$ and the case of helium, respectively. For the case of $(Z, \xi) = (1, 1)$ (figure 5), there is a torus in $\mathcal{D}_1$. The simple stable orbits (the torus) may correspond to the Schubart orbits in the celestial problem (Schubart 1956). Therefore, we call these stable orbits the S-orbits. In the context of atomic physics, it is usually called the asymmetric stretch orbit, which was found by Simonovic and Rost (2001). In figure 5, the region of the torus (S-orbits) is shown as a triangular area located at $\theta = \pi/2$. For the point $\mathbf{z}$ in this triangular area, it is shown that $\chi^{(+)}(\mathbf{z}) = 1 \cdot (21)^{\infty}$. In figure 5, we show the regions of the points $\mathbf{z}$ whose symbol sequence is $\Xi_6(\chi^{(+)}(\mathbf{z})) = 1 \cdot 2n_1n_2 \ldots n_6$, where $n_i \in \mathbf{A}_0\,(i = 1, 2, \ldots, 6)$. There exist missing regions of the points $\mathbf{z}$ whose symbol sequence $\Xi_l(\chi^{(+)}(\mathbf{z}))$ includes the words 1122 and 2211. Our numerical calculation up to the word length 15 has shown that the inadmissible words are only

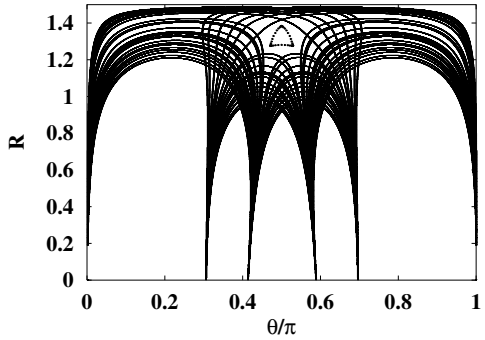

Figure 7. The triple collision curves $\mathcal{C}_{\rm TC}$ and $\mathcal{C}^t_{\rm TC}$ for the case of $(Z, \xi) = (1, 1)$: we also plot the torus region (triangle area). These curves are obtained from the data of figure 5.

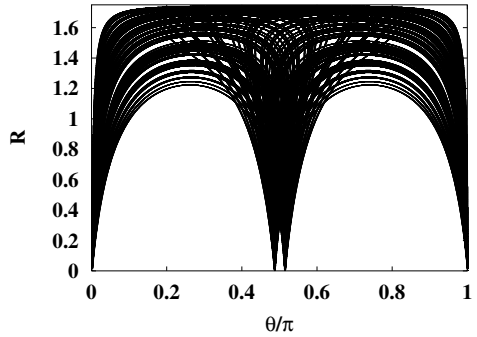

Figure 8. The triple collision curves $\mathcal{C}_{\rm TC}$ and $\mathcal{C}^t_{\rm TC}$ for the case of the helium: these curves are obtained from the data of figure 6.

the words including the words 1122 and 2211. Note that 1122 and 2211 are also inadmissible words for the celestial problem (the case of $(Z, \xi) = (-1, 1)$) and other inadmissible words exist (Tanikawa and Mikkola 2000). On the other hand, for the case of helium (figure 6), i.e. large ξ, there is no torus. Figure 6 shows the regions of the points $\mathbf{z}$ whose symbol sequence is $\Xi_6(\chi^{(+)}(\mathbf{z})) = 1 \cdot 2n_1n_2 \ldots n_6$, where $n_i \in \mathbf{A}_0$ $(i = 1, 2, \ldots, 6)$. In this case, there are no missing regions (i.e. no inadmissible words). When the symbol sequences $1.2n_1 \ldots n_l$ with length $l + 2$ are considered, $\mathcal{D}_1$ is divided into 2^l partitions.

In order to examine the hyperbolicity of the system, we investigate the foliated structure of $\mathcal{D}_1$. Using the second symmetry of $\mathcal{D}_1$, we construct the triple collision curves whose orbit is started at triple collision in the past. We denote the triple collision curves obtained in this way by $\mathcal{C}^t_{\rm TC}$. Figures 7 and 8 depict the triple collision curves whose orbit is started and/or ended at triple collision for the case of $(Z, \xi) = (1, 1)$ and the case of helium, respectively. Figures 7 and 8 are constructed from figures 5 and 6. It is clearly seen that for figure 8 $\mathcal{C}_{\rm TC}$ and $\mathcal{C}^t_{\rm TC}$ transversely cross each other, while for figure 7 $\mathcal{C}_{\rm TC}$ and $\mathcal{C}^t_{\rm TC}$ transversely cross each other except near the torus. Since the dynamics of our system is continuous, we expect that $\mathcal{C}_{\rm TC}$ and $\mathcal{C}^t_{\rm TC}$ do not cross the stable and unstable manifolds. For a discontinuous system, such as a billiard system, this is not the case. In fact, it is numerically confirmed that when ξ is sufficiently large, the triple collision curves $\mathcal{C}_{\rm TC}$ and $\mathcal{C}^t_{\rm TC}$ are parallel to the stable and unstable manifolds, respectively, in the Poincaré section for the Poincaré map. Therefore, figure 8 (sufficiently large ξ) manifests that the dynamics of helium in the collinear eZe configuration

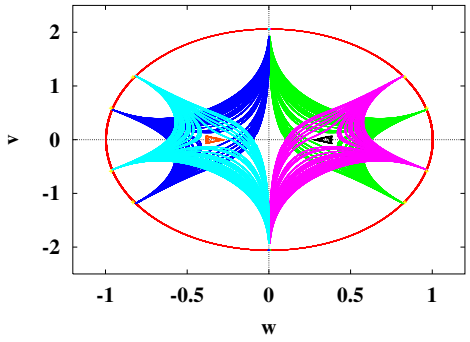

Figure 9. The Poincaré plot of the triple collision orbits $\mathcal{C}_{\rm TC}$ and $\mathcal{C}^t_{\rm TC}$ in (v, w)-coordinates for $(Z, \xi) = (1, 1)$. It corresponds to figure 7.

is hyperbolic. With some parameter values when the torus exists (for small value of ξ), $\mathcal{C}_{\rm TC}$ and $\mathcal{C}^t_{\rm TC}$ do not foliate. In this case, we observe the tangency of $\mathcal{C}_{\rm TC}$ and $\mathcal{C}^t_{\rm TC}$. This may manifest the tangency of the stable and unstable manifolds.

The relationship between the observation in the previous section and the observation in figures 7 and 8 is unclear at present. Next we clarify this relation by transforming the Poincaré plot in (θ, R)-coordinates into that in (s, v, w)-coordinates. The Poincaré surface section in (s, v, w)-coordinates corresponding to that in (θ, R)-coordinates is just the plane $s = 0$. The transformation from (θ, R) to (v, w) is as follows

$$\begin{aligned} v &= \frac{1}{\sqrt[4]{2}}(P_1' + P_2')\sqrt{2 - \frac{1}{2Z} - R} \\ w &= \sqrt[4]{2}\left[2\sqrt{2}\left(2 - \frac{1}{2Z}\right)\right]^{-1/2} \mathbf{s}^T A^T \mathbf{p}' \sqrt{2 - \frac{1}{2Z} - R} \end{aligned} \tag{22}$$

where

$$P_1' = \cos\theta + \sqrt{\frac{\xi}{\xi + 2}}\sin\theta \qquad P_2' = \cos\theta - \sqrt{\frac{\xi}{\xi + 2}}\sin\theta \tag{23}$$

and

$$\mathbf{p}' = \begin{pmatrix} -P_1' \\ P_1' - P_2' \\ P_2' \end{pmatrix} \qquad \mathbf{s} = \frac{1}{\sqrt{2}}\begin{pmatrix} -1 \\ 0 \\ 1 \end{pmatrix}. \tag{24}$$

Figure 9 shows the Poincaré plot of the triple collision orbits in (v, w)-coordinates, which corresponds to figure 7 in (θ, R)-coordinates for $(Z, \xi) = (1, 1)$. $w \geqslant 0$ and $w \leqslant 0$ correspond to $\mathcal{D}_1$ and $\mathcal{D}_2$, respectively. First, we note that there is a special solution along the line $s = w = 0$, which starts from the critical point d and ends in c. It is given by

$$v = -v_c \tanh\left(\frac{\lambda}{2}(\tau - \tau_0)\right) \qquad r = \frac{v_c^2}{2}\,\mathrm{sech}^2\left(\frac{\lambda}{2}(\tau - \tau_0)\right) \tag{25}$$

where τ_0 is determined by the initial condition. This solution shows that $\mathcal{W}^{s,*}(c)$ and $\mathcal{W}^{u,*}(d)$ are degenerated. This type of solution also appears in the symmetric gravitational four-body problem (Sekiguchi and Tanikawa 2002). A second remarkable point is that the triple collision curve $\mathcal{C}_{\rm TC}$ and its reversed pair $\mathcal{C}^t_{\rm TC}$ accumulate at ten points on the TCM (i.e. $w^2 + W(0)^{-1}v^2 = 1$). Figure 10 for $(Z, \xi) = (1, 1)$ shows one branch of $\mathcal{W}_{\rm TCM}(c)$. As

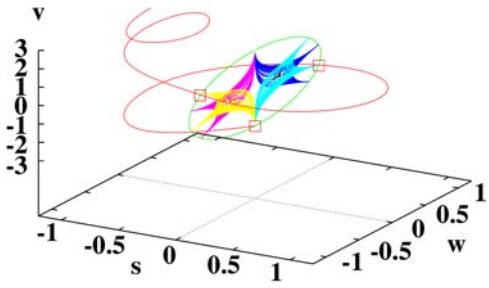

Figure 10. The Poincaré plot of the triple collision orbits and one branch of the unstable manifold of the critical point c for $(Z, \xi) = (1, 1)$. Three crossing points (including the critical point c) where the unstable manifold crosses the Poincaré section $s = 0$ are indicated by squares.

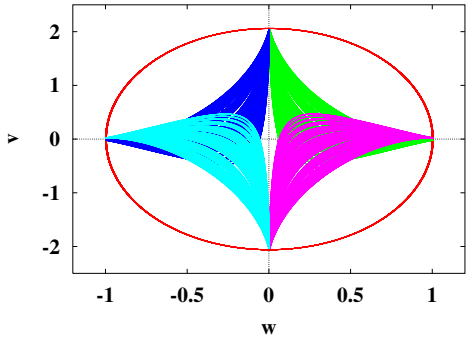

Figure 11. The Poincaré plot of the triple collision orbits $\mathcal{C}_{\mathrm{TC}}$ and $\mathcal{C}^t_{\mathrm{TC}}$ for $(Z, \xi) = (1, 7)$ in (v, w)-coordinates.

shown in figure 10, these points are the points at which $\mathcal{W}_{\mathrm{TCM}}(c)$ and $\mathcal{W}_{\mathrm{TCM}}(d)$ cross the plane $s = 0$. We denote these points by $\mathcal{P}_{TCM,r=0}$. It is easily understood that the number of points of $\mathcal{P}_{TCM,r=0}$ is related to the existence of the tori in the Poincaré surface of section $s = 0$. If the tori exist, its outermost torus has periodic points. These periodic points have stable and unstable manifolds. Some branches of these stable and unstable manifolds run toward $\mathcal{W}_{\mathrm{TCM}}(c)$ and $\mathcal{W}_{\mathrm{TCM}}(d)$. Therefore, the number of points of $\mathcal{P}_{TCM,r=0}$ is directly related to the period of the periodic points associated to the tori. At the same time, the number of points of $\mathcal{P}_{TCM,r=0}$ just corresponds to the winding number $\mathcal{N}$ of $\mathcal{W}_{\mathrm{TCM}}(c)$ or $\mathcal{W}_{\mathrm{TCM}}(d)$ around the body of the TCM, as observed in the previous section. In figure 11, the case of $(Z, \xi) = (1, 7)$ is shown. As the result of the previous section, when ξ is large enough, the winding number of $\mathcal{W}_{\mathrm{TCM}}(c)$ and $\mathcal{W}_{\mathrm{TCM}}(d)$ saturates to a certain value. In other words, when ξ is large enough, the number of points of $\mathcal{P}_{TCM,r=0}$ also saturates to a certain value which is, in fact, six (i.e. no torus case). Thus, the existence of a torus in the Poincaré section $s = 0$ is monitored by the number of points of $\mathcal{P}_{TCM,r=0}$. When ξ is large enough, the triple collision curve $\mathcal{C}_{\mathrm{TC}}$ transversely crosses $\mathcal{C}^t_{\mathrm{TC}}$. This would be strong evidence of hyperbolicity of the system with large ξ, since it is numerically confirmed that $\mathcal{C}_{\mathrm{TC}}$ and $\mathcal{C}^t_{\mathrm{TC}}$ are parallel to the stable and unstable manifolds, respectively, for the Poincaré map.

The critical value of $\xi_c(Z)$ at which the winding number $\mathcal{N}$ is minimized, is calculated. In table 1, we summarize the result. For $Z = 1, 2, 3, 4, 5$, the critical value $\xi_c(Z)$ is of the order of $O(10)$. The critical value is numerically obtained. Thus, these are not true critical values. However, we expect that, at these true critical values, the unstable manifold of c and

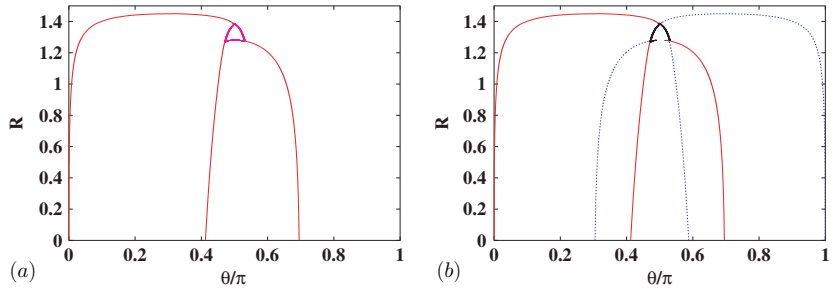

Figure 12. The stable and unstable manifolds of α, β and γ for the case of $(Z, \xi) = (1, 1)$: (a) the stable manifolds of α, β and γ, (b) the unstable manifolds (dotted lines) of α, β and γ are also added to (a).

Table 1. The critical value $\xi_c(Z)$.

Z	$\xi_c(Z)$
1	6.4
2	15.0
3	23.5
4	32.0
5	40.4

the stable manifold of d degenerate. At the critical value $\xi_c(Z)$, the tori disappear. At present, we do not know the precise mechanism of this disappearance of the tori, e.g., despite whether the KAM scenario is applied or not.

From the above numerical observation, we can state a conjecture. For the system equation (4) with (Z, ξ), there exists the critical value $\xi_c(Z)$ such that for $\xi > \xi_c(Z)$ the system is hyperbolic.

Since for the actual two-electron atom or ions the mass ratio is large, i.e. $m_p/m_e \approx 1840$, this means that the classical dynamics of H^-, He, Li^+, $Be^{2+}, \ldots,$ in the collinear eZe configuration is hyperbolic. For infinite mass ratio, it has been shown numerically that the symbolic description is complete and the dynamics probably hyperbolic (Bai *et al* 1998).

4.1. The case of $(Z, \xi) = (1, 1)$

In this subsection, we investigate the detailed structure of the Poincaré surface of section for the case of $(Z, \xi) = (1, 1)$. In this case, there is a torus whose symbol sequence is $1 \cdot 21212\ldots$ as shown in figures 5 and 7. This torus has the periodic points with period 6 as the outermost part. Note that we include the periodic points in $\mathcal{D}_2$ and count the period. These periodic points α, β, γ have stable and unstable manifolds: $\alpha : (\theta, R) = (0.5\pi, 1.385)$, $\beta : (\theta, R) = (0.5292\pi, 1.275)$ and $\gamma : (\theta, R) = (0.4708\pi, 1.275)$. From the numerical calculation, one branch of $\mathcal{W}^s(\alpha)$ is equal to one branch of $\mathcal{W}^u(\beta)$. In the same way, one branch of $\mathcal{W}^s(\beta)$ is equal to one branch of $\mathcal{W}^u(\gamma)$ and one branch of $\mathcal{W}^s(\gamma)$ is equal to one branch of $\mathcal{W}^u(\alpha)$. We can construct the stable manifolds of α, β and γ outside the S-orbits by examining the long orbits with the symbol sequence $1 \cdot 21212\cdots$. The result is depicted in figure 12(a). In figure 12(b), we also depict the unstable manifolds by using the second symmetry of $\mathcal{D}_1$. The stable manifolds of α, β and γ outside the S-orbits are basic boundaries of the partitions of $\mathcal{D}_1$.

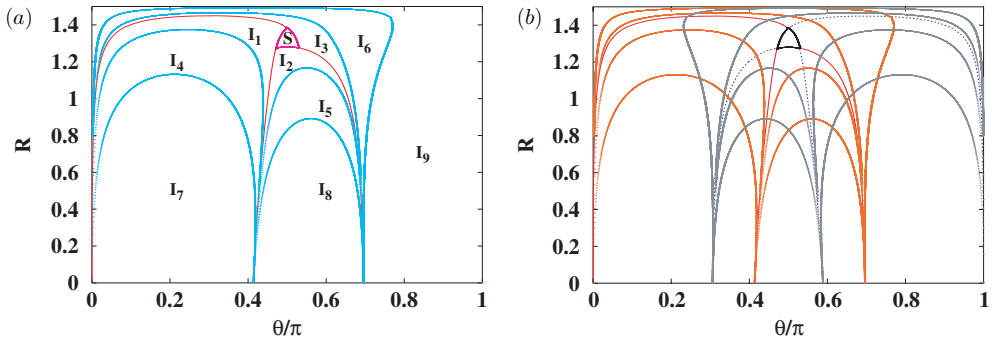

Figure 13. The partitions in $\mathcal{D}_1$ for the case of $(Z, \xi) = (1, 1)$: (a) the partitions in $\mathcal{D}_1$, (b) the time-reversed partitions are also added to (a).

Table 2. The characteristic feature of each partition for $(Z, \xi) = (1, 1)$.

Partition	Character	Symbol sequence
S	S-orbits(torus)	$1 \cdot (21)^{\infty}$
I_1		$1 \cdot (21)^n \ldots (n \geqslant 2)$
I_2		$1 \cdot (21)^n \ldots (n \geqslant 2)$
I_3		$1 \cdot (21)^n \ldots (n \geqslant 2)$
I_4		$1 \cdot (2)^n 12 \ldots (n \geqslant 2)$
I_5		$1 \cdot 2(1)^n 21 \ldots (n \geqslant 2)$
I_6		$1 \cdot 21(2)^n 12 \ldots (n \geqslant 2)$
I_7	Escape	$1 \cdot (2)^{\infty}$
I_8	Escape	$1 \cdot 2(1)^{\infty}$
I_9	It is mapped to I_7	$1 \cdot 21(2)^{\infty}$

We have further examined the symbol sequence $\Xi_{60}(\chi^{(+)}(\mathbf{z}_{mn}))$ for each $\mathbf{z}_{mn}$ $(0 \leqslant m \leqslant 1800, 0 \leqslant n \leqslant 1000)$. As a result, $\mathcal{D}_1$ is divided into, at least, ten partitions: $S, I_i\ (i = 1, 2, \ldots, 9)$. S denotes the S-orbits. Other partitions $I_i\ (i = 1, 2, \ldots, 9)$ are defined as follows. We examined the symbol sequences $\Xi_{60}(\chi^{(+)}(\mathbf{z}))$ along the line $\theta = 0.2\pi$, 0.5π, 0.55π and 0.7π. For the line $\theta = 0.2\pi$, we find that the symbol sequences are distributed as it decreases from $1 \cdot (2)^{\infty}$ to $1 \cdot (21)^{\infty}$ with increasing R. We divide symbol sequences into three groups: $1 \cdot (2)^{\infty}$, $1 \cdot (2)^n 12 \ldots$ and $1 \cdot (21)^n \ldots (n \geqslant 2)$. We call the regions with these symbol sequences I_7, I_4 and I_1, respectively.

For the line $\theta = 0.5\pi$, the symbol sequences are distributed as it increases from $1 \cdot 2(1)^{\infty}$ to $1 \cdot (21)^{\infty}$. We divide symbol sequences into three groups: $1 \cdot 2(1)^{\infty}$, $1 \cdot 2(1)^n 21 \ldots$ and $1 \cdot (21)^n \ldots (n \geqslant 2)$. We call the regions with these symbols sequences I_8, I_5 and I_2, respectively.

By examining the symbol sequences along the line $\theta = 0.55\pi$ and 0.7π, we find that along the line $R = 1.3$ from $\theta = \pi$ to 0.5π, the symbol sequences are distributed as it decreases from $1 \cdot 21(2)^{\infty}$ to $1 \cdot (21)^{\infty}$ with decreasing θ. We divide symbol sequences into three groups: $1 \cdot 21(2)^{\infty}$, $1 \cdot 21(2)^n 12 \ldots$ and $1 \cdot (21)^n \ldots (n \geqslant 2)$. We call the regions with these symbols sequences I_9, I_6 and I_3, respectively. Figure 13(a) shows these partitions of $\mathcal{D}_1$. In figure 13(b), the time-reversed partitions by the second symmetry of $\mathcal{D}_1$ are shown with those of figure 13(a). In table 2, the characteristic features of S and $I_i\ (i = 1, 2, \ldots, 9)$ are summarized.

Next we prepared many points in each partition and checked which partitions they are mapped to. In table 3, we summarize the transition among the partitions. From table 3, we

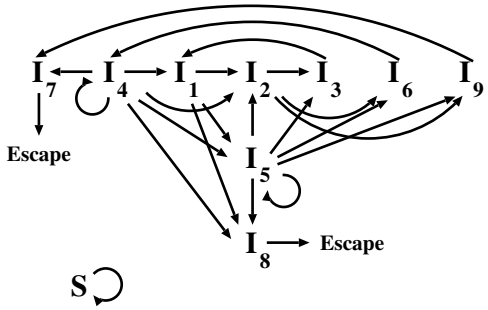

Figure 14. The transition diagram for the case of $(Z, \xi) = (1, 1)$ among the partitions derived from table 2.

Table 3. The transitions among the partitions for $(Z, \xi) = (1, 1)$.

Transitions
$S \to S$
$I_1 \to I_2, I_5, I_8$
$I_2 \to I_3, I_6, I_9$
$I_3 \to I_1$
$I_4 \to I_1, I_2, I_4, I_5, I_7, I_8$
$I_5 \to I_2, I_3, I_5, I_6, I_8, I_9$
$I_6 \to I_4$
$I_7 \to$ Escape
$I_8 \to$ Escape
$I_9 \to I_7$

have drawn the diagram of the transitions among partitions in figure 14. From this diagram, we know that typical orbits travel around the regions near the torus (I_1, I_2 and I_3) and/or around the regions in which the orbits feel large instability (I_4, I_5 and I_6) and that, in most cases, they escape to the regions (I_7, I_8 and I_9) except the S-orbits and non-wandering orbits (probably repellor).

4.2. The case of helium

For the case of helium, figures 6 and 8 show all features of the partitions. The partitions formed by $\mathcal{C}_{\mathrm{TC}}$ are, at first sight, expected to be Markov partitions. If we obtain $\mathcal{C}_{\mathrm{TC}}$ using the symbol sequences $1.2n_1 \ldots n_l$, then $\mathcal{D}_1$ is divided into 2^l partitions. From numerical observation, there are no inadmissible words. However, it is clear that $\bar{1}$ and $\bar{2}$ are removed, since these orbits correspond to fixed points at infinity. The Markov partition should be shaped as a parallelepiped. Thus probably, in a mathematically rigorous sense, the partitions in our Poincaré section are not Markov partitions. If we construct the Markov partitions in our Poincaré section, they would be infinite. This reflects the fact that the dynamics of the helium atom in the collinear eZe configuration exhibits intermittency (Richter *et al* 1993, Tanner and Wintgen 1995, Tanner *et al* 2000). The intermittency observed in the helium atom in the collinear eZe configuration is the behaviour in which the electrons go back and forth between long flight (i.e. almost ionization) and short flight (i.e. successive collisions with the nucleus). This intermittency is due to the existence of the fixed points at infinity. Its behaviour

is very similar to the hyperbola billiard (Sieber and Steiner 1990). The transverse crossing of $\mathcal{C}_{\rm TC}$ and $\mathcal{C}^t_{\rm TC}$ strongly suggests that the dynamics is hyperbolic.

4.3. The Poincaré plots for other two-electron ions

Bai *et al* (1998) have investigated the case of the infinite nucleus mass. It was numerically shown that, for $Z \geqslant 1$, the symbolic description is complete and this suggests that the system is hyperbolic. We now consider the finite mass case. The investigation above does not consider the Z dependence of the dynamics of the two-electron atom and ions in the collinear eZe configuration. Now, in order to strengthen our claim that their dynamics are fully chaotic, probably hyperbolic, we calculate the Poincaré plots for 30 atoms and ions among the systems H^-, He, Li^+, ..., Fm^{98+} in the collinear eZe configuration. Due to constrictions on the length of the paper, we do not plot them. This calculation shows that, even though Z becomes large at the order of $O(100)$ and then the interaction terms become small in equation (8), their large mass ratio ξ overcomes the Z dependence to result in the fact that the Poincaré plot is filled by a chaotic sea except for the escape region, and there is no visible torus. These observations strengthen our claim.

5. Experimental aspect

From our observations, we know that the system with small mass ratio qualitatively differs from the system with large mass ratio, namely the existence of stable orbits. This difference can be experimentally observed. Possible candidates are the antiproton–proton–antiproton ($\overline{\rm p}$–p–$\overline{\rm p}$) system, the positronium negative ion (Pr-(e–$\overline{e}$–e)). which corresponds to the case of $Z = 1, \xi = 1$. We neglect relativistic effects, bremsstrahlung and hyperfine interaction. If this system has bound states, the eigenenergies possess the effects of the torus. The most convenient analysis is the Fourier transform of the density of states for the spectrum with the angular momentum $\mathbf{L} = 0$, which gives information on the length and the stability of periodic orbits. For the positronium negative ion, the EBK quantization was performed (Simonovic and Rost 2001). A stable antisymmetric orbit was obtained and was quantized to explain the energy spectrum. From our observation, as a ZeZ configuration, the positive hydrogen molecule H_2^+ has stable periodic orbits.

In addition, although large Z two-electron ions are experimentally unrealistic, small Z two-electron ions provide us with the data for the manifestation of our finding; i.e. hyperbolicity (strong chaotic property). H^- and He have been already analysed by the semiclassical method (Gaspard and Rice 1993, Ezra *et al* 1991). Therefore, Li^+ is another candidate. If we change Z, the degree of the intermittency of the dynamics would change (Tanner and Wintgen 1995). This change may be reflected in the behaviour of the quantum defect of H^-, He, Li^+, Be^{2+}, ...

6. Summary

In this paper, we have investigated the bifurcation in the classical Coulomb three-body problem in the collinear eZe configuration with the finite mass of all three particles. In particular, the main result is that, when the mass ratio ξ is changed, the change of the flow on the TCM is directly related to the existence (or collapse) of the tori. This result suggests that if the mass ratio ξ is sufficiently large, the dynamics of these systems is hyperbolic. This result is consistent with the result (i.e. infinite nucleus mass) by Bai *et al* (1998). However, using our analysis, it is shown that there surely exists a threshold value of ξ for hyperbolicity. This threshold value is of the order of $O(10)$. Therefore, H^-, He, Li^+, Be^{2+}, ..., in the collinear

eZe configuration are hyperbolic. Since our analysis is based on a numerical analysis, we do not have any proof of this fact. We call for rigorous proof of this result.

Acknowledgment

The author is grateful to Professor K Tanikawa for stimulating discussion on the three-body problem in celestial mechanics.

Appendix

In this appendix, we derive the TCM for our Coulomb systems. Its derivation is completely parallel to the case of the celestial problem. We recommend that readers consult the paper by McGehee (1974) for further details. We start from the Hamiltonian equation (4)

$$\mathcal{H} = T(\mathbf{p}) - U(\mathbf{q}) = E \tag{A.1}$$

where we removed the dash in equation (4). $T(\mathbf{p})$ is the kinetic part of $\mathcal{H}$ and $-U(\mathbf{q})$ is the potential part of $\mathcal{H}$. The equations of motion in the Cartesian coordinates are given by

$$\frac{\mathrm{d}\mathbf{q}}{\mathrm{d}t} = M^{-1}\mathbf{p} \qquad \frac{\mathrm{d}\mathbf{p}}{\mathrm{d}t} = \nabla U(\mathbf{q}) \tag{A.2}$$

with the mass matrix

$$M = \begin{bmatrix} 1 & 0 & 0 \\ 0 & \xi & 0 \\ 0 & 0 & 1 \end{bmatrix}. \tag{A.3}$$

We set the centre of mass to be zero:

$$q_1 + \xi q_2 + q_3 = 0. \tag{A.4}$$

We set the total momentum to be also zero:

$$p_1 + p_2 + p_3 = 0. \tag{A.5}$$

We consider the transformation from the Cartesian coordinates $(q_1, q_2, q_3, p_1, p_2, p_3)$ with equations (A.4) and (A.5) to the McGehee variables (r, s, v, w). First, we set

$$r = (\mathbf{q}^T M \mathbf{q})^{1/2} \qquad \mathbf{s} = r^{-1}\mathbf{q} \tag{A.6}$$

where r^2 is the moment of inertia and $\mathbf{s}$ represents the configuration of three particles. The triple collision corresponds to $r = 0$. Now we parametrize the variable $\mathbf{s}$ by single variable s. To do so, we set

$$\begin{aligned} &\mathbf{a} = (a_1, a_2, a_3) \qquad a_1 = a_2 < a_3 \\ &\mathbf{b} = (b_1, b_2, b_3) \qquad b_1 < b_2 = b_3 \end{aligned} \tag{A.7}$$

where

$$\mathbf{a}^T M \mathbf{a} = \mathbf{b}^T M \mathbf{b} = 1. \tag{A.8}$$

Since we fix the centre of mass, namely $a_1 + \xi a_2 + a_3 = 0$ and $b_1 + \xi b_2 + b_3 = 0$, then we have

$$\begin{aligned} \mathbf{a} &= \left(-\frac{1}{\sqrt{(1+\xi)(2+\xi)}}, -\frac{1}{\sqrt{(1+\xi)(2+\xi)}}, \frac{1+\xi}{\sqrt{(1+\xi)(2+\xi)}} \right) \\ \mathbf{b} &= \left(-\frac{1+\xi}{\sqrt{(1+\xi)(2+\xi)}}, \frac{1}{\sqrt{(1+\xi)(2+\xi)}}, \frac{1}{\sqrt{(1+\xi)(2+\xi)}} \right). \end{aligned} \tag{A.9}$$

It is shown that the variable $\mathbf{s}$ is parametrized by the variable $s \in [-1, 1]$ as follows (see McGehee (1974) for details)

$$\mathbf{s} = (\sin(2\lambda))^{-1} [\sin(\lambda(1-s)\mathbf{a} + \sin(\lambda(1+s))\mathbf{b}] \tag{A.10}$$

with

$$\cos(2\lambda) = \mathbf{a}^T M \mathbf{b} = \frac{1}{1+\xi}. \tag{A.11}$$

Here λ is valued as $0 \leqslant \lambda \leqslant \pi/2$. We denote the map from $s \in [-1, 1]$ to the configuration $\mathbf{s}$ by S:

$$\begin{array}{rccl} S: & [-1,1] & \to & \{\mathbf{s} : \mathbf{s}^T M \mathbf{s} = 1, s_1 + \xi s_2 + s_3 = 0\} \\ & s & \mapsto & \mathbf{s}. \end{array} \tag{A.12}$$

Note that $s = -1$ ($s = 1$) corresponds to the collision of the particles 1 and 2 (2 and 3). $U(\mathbf{s})$ becomes

$$\begin{aligned} V(s) &= U(S(s)) \\ &= \sin(2\lambda) \left[\frac{1}{(b_2 - b_1)\sin(\lambda(1+s))} + \frac{1}{(a_3 - a_2)\sin(\lambda(1-s))} \right. \\ &\quad \left. - \frac{1}{Z\{(b_2 - b_1)\sin(\lambda(1+s)) + (a_3 - a_2)\sin(\lambda(1-s))\}} \right]. \end{aligned} \tag{A.13}$$

Here we set two matrices A_1 and A_2

$$A_1 = \begin{bmatrix} 1 & 1 & 1 \\ 1 & 1 & 1 \\ 1 & 1 & 1 \end{bmatrix} \qquad A_2 = \begin{bmatrix} 0 & 1 & -1 \\ -1 & 0 & 1 \\ 1 & -1 & 0 \end{bmatrix} \tag{A.14}$$

and define the matrix A

$$A = \frac{1}{2+\xi} A_1 M + \left(\frac{\xi}{2+\xi} \right)^{1/2} M^{-1} A_2. \tag{A.15}$$

Now the variable s is defined as the inverse of equation (A.10):

$$s = S^{-1}(\mathbf{s}). \tag{A.16}$$

We further set

$$v = r^{1/2} \mathbf{p}^T \mathbf{s} \qquad w = r^{1/2}(1-s^2) W(s)^{-1/2} \mathbf{s}^T A^T \mathbf{p} \tag{A.17}$$

where

$$W(s) = 2(1-s^2)V(s). \tag{A.18}$$

We also employ time-transformation two times:

$$\mathrm{d}t = r^{3/2}\,\mathrm{d}t' \qquad \text{and} \qquad \mathrm{d}t' = \lambda(1-s^2)W(s)^{-1/2}\,\mathrm{d}\tau. \tag{A.19}$$

In short, the change of variable equations (A.6), (A.16), (A.17) and (A.19) give the desired relations, i.e. the energy conservation and the equations of motion. The energy conservation becomes

$$1 - \frac{2w^2}{1-s^2} = \frac{2(1-s^2)}{W(s)}(v^2 - 2rE) - 1. \tag{A.20}$$

The equations of motion become

$$\begin{aligned}
\frac{\mathrm{d}r}{\mathrm{d}\tau} &= \frac{\lambda(1-s^2)}{W(s)^{1/2}} r v \\
\frac{\mathrm{d}v}{\mathrm{d}\tau} &= \frac{\lambda}{2} W(s)^{1/2} \left[1 - \frac{1-s^2}{W(s)} (v^2 - 4rE) \right] \\
\frac{\mathrm{d}s}{\mathrm{d}\tau} &= w \\
\frac{\mathrm{d}w}{\mathrm{d}\tau} &= -s + \frac{2s(1-s^2)}{W(s)} (v^2 - 4rE) + \frac{1}{2} \frac{W'(s)}{W(s)} (1 - s^2 - w^2) - \frac{\lambda(1-s^2)}{2W(s)^{1/2}} vw.
\end{aligned} \tag{A.21}$$

Finally, we set $r = 0$. Thanks to the above transformations, this substitution is meaningful, since the singularities from the double collisions have been removed. From equations (A.20) and (A.21), we obtain equations (15) and (16). We can also set $E = 0$. Then the same energy relation and the equations of motion are obtained, since r and E appear as a term rE. The dynamics of scattering flow for $E = 0$ was investigated by Bai *et al* (1998) for the case of the infinite nucleus mass.

References

Bai Z-Q, Gu Y and Yuan J-M 1998 *Physica* D **118** 17
Einstein A 1917 *Verh. Dtsch. Phys. Ges.* **19** 82
Ezra G S, Richter K, Tanner G and Wintgen D 1991 *J. Phys. B: At. Mol. Opt. Phys.* **24** L413
Gaspard P and Rice S A 1993 *Phys. Rev.* A **48** 54
Gutzwiller M C 1971 *J. Math. Phys.* **12** 343
Gutzwiller M C 1990 *Chaos in Classical and Quantum Mechanics* (New York: Springer)
McGehee R 1974 *Invent. Math.* **27** 191
Mikkola S and Tanikawa K 1999 *Celest. Mech. Dyn. Astron.* **74** 287
Mikkola S and Tanikawa K 1999 *Mon. Not. R. Astron. Soc.* **310** 745
Siegel C L and Moser J K 1971 *Lectures on Celestial Mechanics* (Berlin: Springer)
Poincaré H 1899 *Les méthodes nouvelles de la méchanique céleste I, II et III* (Paris: Gauthier-Villars)
Richter K, Tanner G and Wintgen D 1993 *Phys. Rev.* A **48** 4182
Schubart J 1956 *Astron. Nachr.* **283** 17
Sekiguchi M and Tanikawa K 2002 On the symmetric collinear four-body problem *Preprint*
Sieber M and Steiner F 1990 *Physica* D **44** 248
Simonovic N and Rost J-M 2001 *Eur. Phys. J.* D **15** 155
Tanikawa K and Mikkola S 2000 *Chaos* **10** 649
Tanner G, Richter K and Rost J-M 2000 *Rev. Mod. Phys.* **72** 497
Tanner G and Wintgen D 1995 *Phys. Rev. Lett.* **75** 2928
Yoshida H 1990 *Phys. Lett.* A **150** 262